Velocity Imaging Studies on Ion−Pair Dissociation of CH3Br + hνVUV → CH3+ + Br− as a Function of Wavelengthth†

ARTICLE *in* THE JOURNAL OF PHYSICAL CHEMISTRY A · SEPTEMBER 2004

Impact Factor: 2.69 · DOI: 10.1021/jp048063h

3 AUTHORS, INCLUDING:

WIlliam M. Jackson
University of California, Davis
234 PUBLICATIONS **2,631** CITATIONS

Velocity Imaging Studies on Ion-Pair Dissociation of $CH_3Br + h\nu_{VUV} \rightarrow CH_3^+ + Br^-$ as a Function of Wavelength†

Dadong Xu, Jianhua Huang, Roosevelt J. Price, and William M. Jackson*

Department of Chemistry, University of California, Davis, California 95616

Received: May 5, 2004; In Final Form: August 12, 2004

The ion-pair dissociation dynamics of $CH_3Br + h\nu_{VUV} \rightarrow CH_3^+ + Br^-$ as a function of vacuum ultraviolet (VUV) wavelength have been studied by means of velocity imaging. Photofragment excitation (PHOFEX) spectra as well as images for both the cation and the anion products have been collected, which confirm the dissociation occurs through the ion-pair channel from the momentum matching of both products. The wavelength region for the PHOFEX covers a small portion (from 121.4 to 122.7 nm) of the absorption spectrum where transitions from the ground state to both ns and np Rydberg states as well as to the underlying continuum states are all present. Images were taken at selected wavelengths both on the peaks and in the valleys of the PHOFEX spectrum, as well as at 118.22 nm. The PHOFEX spectra closely resemble the absorption spectra of CH_3Br, and the images taken at peaks and continuum wavelengths in PHOFEX show no marked differences with respect to the product energy and angular distributions. These observations prompt us to conclude that the ion-pair state is directly populated by the VUV photons and the ion-pair dissociation is one of the major exit channels for the excited states in the energy region just below the ionization energy of the parent molecule, although large uncertainties in wavelength in the absorption spectra make the proposed mechanisms less conclusive.

I. Introduction

Molecular ion-pair states are the excited electronic states of molecules that are formed when a cation and an anion are brought together. Dissociation from these states leads to pairs of positive and negative ions in the diabatic representation. In this description, the negative charge is localized in the assigned orbitals of the negative ion, and there is no significant electron exchange throughout the entire internuclear separation (R). Because of electron localization, the energy curve can be fairly well described with Coulombic attraction at $R \geq R_e$, the equilibrium internuclear distance, which is usually larger than that for valence states and Rydberg states. At shorter R, an exponential decay term can be used to describe the repulsion between the two ions. The potential energy curve for the lowest ion-pair state can be expressed as[1]

$$V(R) = A \exp(-\alpha R) - e^2/(4\pi\epsilon_0 R) + D_e(AB) + E_i(A) - E_{ea}(B) \quad (1)$$

for $AB \rightarrow A^+ + B^-$, where both ions are in their ground states. $D_e(AB)$ is the dissociation energy for forming neutral fragments $A + B$. E_i and E_{ea} represent the ionization energy (IE) and the electron affinity (EA) for A and B, respectively. The ion pair dissociation threshold can be estimated using the last three terms in eq 1. However, strong interactions between ion-pair states and Rydberg and valence states will dramatically change the simple picture of the potential energy curves, eq 1. The crossings now become avoided and the resulting adiabatic curves may have double wells, with the inner well being mainly of Rydberg character.

Photoinduced ion-pair formation has been studied for many years. In a review paper, Berkowitz compiled many molecules from which ion-pair dissociation was observed.[2] Relative efficiencies, observed and calculated thresholds, and some generalizations were given for ion-pair processes. These processes are particularly easy to initiate in halogen-containing molecules because the large EA of the halogen atom will significantly lower the threshold for the ion-pair production. As a result, the ion-pair dissociation thresholds for most halogenated molecules are below the IE of the molecules. At energies above the IE, the probability decreases for ion-pair production because of the competition from direct ionization. In some cases, the ion-pair productions have been compared with the absorption spectra of the molecules, and it has been shown that they are similar to each other.[2,3] It is suggested that the Rydberg states and the nearby valence states initially excited are strongly coupled to the ion-pair continuum, assuming that the ion-pair states are not directly accessible because of the large displacement of these states.

Due to the nature of Coulombic attraction between cation and anion at large internuclear distance, vibrational levels can be very high within ion-pair states. This is analogous to high n Rydberg states which usually have long lifetimes in the microsecond time scale. In case of I_2, vibrational levels as high as $v > 600$ have been observed by means of resonance enhanced multiphoton ionization.[4] In recent years, high-resolution spectroscopic studies on ion-pair states have been performed to determine precise ion-pair dissociation limits and bond dissociation energies for neutral products.[5,6] In these studies, a pulsed DC field was used after a certain delay relative to the excitation laser pulse to induce the threshold ion-pair dissociation. Hepburn and co-workers termed the method as threshold ion-pair production spectroscopy (TIPPS)[7,8] and successfully applied it to a number of molecular systems, whereas Donovan

† Part of the special issue "Tomas Baer Festschrift".

* To whom correspondence should be addressed. E-mail: wmjackson@ucdavis.edu.

10.1021/jp048063h CCC: $27.50
Published on Web 09/28/2004

and co-workers called it zero ion kinetic energy (ZIKE)[5] spectroscopy because of the exact analogy to the previously known zero electron kinetic energy (ZEKE)[9] spectroscopy. In TIPPS or ZIKE, the ions from prompt dissociation were allowed to escape during the delay period so that the signals arose from the ions produced by the subsequent pulsed field. One should note that those prompt ions contain dynamics information which was discarded in spectroscopic studies when the excitation energy is above the dissociation limit of the lowest ion-pair state.

Ion-pair yields as a function of wavelength have been measured for some halogenated methanes [2,3,10] both below and above IEs of the molecules. Some of the features could be assigned to specific Rydberg transitions. The ion-pair dissociation dynamics for some alkyl halides (RX, R = CH_3, C_2H_5 and X = Cl, Br) have been reported at fixed wavelengths, mainly 118 nm.[11−13] In all cases, strong anisotropic angular distributions with positive β were observed although the geometries and the initial excited states are different for different molecules. This observation indicates that the transition dipole moment is always parallel to the C−X bond, regardless of the molecular structure (C_{3v} or C_s).

The absorption spectra of CH_3Br in the VUV region have been reported by Causley and Russell[14] and Hochmann et al.[15] The absorption peaks have been assigned to Rydberg states of ns, ns′ and np, np′ series, which result from the excitation of nonbonding 4pπ electron of the molecule to the s and p Rydberg orbitals. The notations of ns and np refer to the ground-state ion core ($^2E_{3/2}$) and ns′ and np′ to the spin−orbit excited ion core ($^2E_{1/2}$). There is also a background continuum underlying the structured Rydberg peaks that can be attributed to highly excited valence states having higher occupancy in antibonding orbitals, σ^*(C−H) and/or σ^*(C−Br). In the present study, we report the ion-pair dissociation dynamics of CH_3Br as a function of VUV wavelength. The wavelength region that is studied covers a portion of the absorption spectrum where ns, np, np′ Rydberg levels as well as the underlying continuum should be present. Both ion images and PHOFEX spectra of the CH_3^+ and Br^- ions have been collected. A close relationship between the absorption and the PHOFEX spectra of both ions has been observed, and the momentum match obtained from the images of these ions confirms that the ion-pair process is occurring.

II. Experimental Section

The ion velocity imaging apparatus has been described in detail elsewhere.[16] It consists of three stainless steel chambers pumped with separate turbo-molecular pumps. The pulsed molecular beam source chamber houses a piezoelectric pulsed valve with a 0.25 mm nozzle. The molecular beam is skimmed and then collimated before it interacts with the laser beam in the reaction chamber. During the experiments, the typical pressure in this chamber is 4×10^{-5} Pa. The laser beam enters the reaction chamber in a direction that is perpendicular to the molecular beam and intercepts the molecular beam in the center of the ion optics for the time-of-flight mass spectrometer (TOF-MS). The ion optics consist of three plates, a repeller, an accelerator, and a ground plate which is the entrance to the flight tube for the mass spectrometer. High voltages of appropriate ratio for ion velocity imaging are applied to the repeller and the accelerator to focus the ions into the flight tube that is perpendicular to the plane defined by the laser and the molecular beams. A typical voltage ratio in our experiment is 1500 V/1042 V. The TOF-MS tube is maintained at a pressure around 8×10^{-7} Pa and allows the ion cloud to fly in a field-free region for 62 cm before it strikes the detector. The detector assembly consists of two stacked microchannel plates (Burle 3040-FM), a fast P47 phosphor screen, a CCD camera (Mintron 2821E) mounted behind the screen to collect images, and a photomultiplier tube to record TOF spectra by monitoring the light from the phosphor screen. The TOF spectra were recorded with a digital oscilloscope (HP 54810A). The original three-dimensional (3D) ion distribution is restored from the raw two-dimensional (2D) image by means of a back-projection program.[17]

Tunable coherent VUV radiation was obtained by frequency tripling the doubled output around 366 nm from a dye laser (Lambda-Physik, Scanmate II) pumped by an Nd:YAG laser (Spectra-Physics, Pro-230−30). A quartz lens was used to focus the UV laser into a VUV cell containing $\sim 3 \times 10^3$ Pa of krypton (Kr). The exit window of this VUV cell is a lithium fluoride (LiF) lens that has focal lengths of ~6 and ~11 cm at 122 and 366 nm, respectively. The focus point of the 366 nm was adjusted at ~6 cm in front of the LiF lens so that it collimated the VUV light and diverged the UV light in the reaction region. The polarization of the UV laser was parallel to the surface of the detector and so was the polarization of the resulting VUV. The typical input energy of 366 nm was about 9 mJ/pulse, which generated less than 90 nJ/pulse of the VUV light (tripling efficiency $<10^{-5}$). There were photoelectrons produced by VUV ionization of background gases and from metal surfaces. To avoid ions produced by electron impact, pulsed voltages of 20 μs duration were applied to the ion optics plates 200 ns after the VUV passed through the chamber. During this delay time, the electrons were allowed to escape the interaction region. It was verified that using pulsed voltages on the ion optics plates did not change the speed and angular distributions of product ions. By scanning the dye laser, the PHOFEX spectra of the CH_3^+ and the Br^- ions were recorded using a Boxcar Averager (SR250). Positive voltages on the ion optics plates were used for detecting CH_3^+, whereas negative voltages of the same ratio were used for detecting Br^-.

Bromomethane (99.5%) was obtained from Matheson and used without further treatment. A neat beam of CH_3Br was formed at a stagnation pressure of 1.33×10^4 Pa at room temperature. Under these expansion conditions, no cluster ions were found in the TOF-MS within the sensitivity of the apparatus when 118 nm photons were used for soft ionization.[18] The TTL trigger for opening the pulsed valve was set to make sure VUV light hit the front part of the molecular beam, which further discriminated against photodissociation of clusters. The procedures of converting speed to energy distribution and the energy scale calibration have been described in an earlier publication.[19] After back-projection, the population as a function of pixels is obtained, which is equivalent to population as a function of speed $P(v)$. This distribution is converted to the translational energy distribution, $P(E_T)$, by using Jacobian transformation $v \rightarrow v^2 \propto E_T$ and $P(v) \rightarrow P(v)/v \propto P(E_T)$. The appropriate voltage ratio for velocity imaging is found by checking the image of the parent ion, which should be tiny and circular under the right focus conditions. From time to time, the voltage on the accelerator may need to be adjusted within a few volts to get the best focusing, but this has little effect on the translational energy distribution.

III. Results

A. Photofragment Excitation Spectra. The threshold for the ion-pair dissociation

$$CH_3Br \rightarrow CH_3^+ + Br^-, \Delta H = 219.2 \text{ kcal/mol} \qquad (2)$$

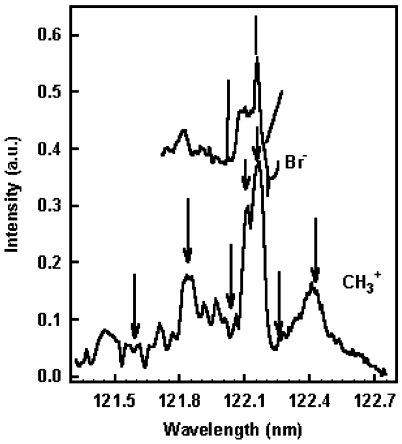

Figure 1. PHOFEX spectra of CH_3^+ (lower curve) and Br^- (upper curve) produced from ion-pair dissociation of CH_3Br. Arrows and lines indicate wavelengths where images were recorded for CH_3^+ and Br^-, respectively. The peaks at 121.83, 122.16, and 122.43 nm can be identified as 7p′, 9s, and 8p Rydberg states, respectively.

can be calculated using the last three terms in eq 1. The heats of formation for CH_3Br (−8.2 kcal/mol), CH_3 (34.8 kcal/mol), and Br (26.7 kcal/mol) and the EA for Br (3.3636 eV) are all taken from the NIST Chemistry Webbook.[20] The adiabatic IE for CH_3 (9.8382 eV) is taken from ref 21. The theoretical threshold wavelength for reaction 2 is 130.43 nm, and the experimental value is 130.5 nm.[2]

Figure 1 shows the PHOFEX spectra of CH_3^+ and Br^- ions formed from ion-pair dissociation of CH_3Br, eq 2. From the absorption spectrum of Causley and Russell,[14] the peaks at 121.83, 122.16, and 122.43 nm can be identified as 7p′, 9s, and 8p Rydberg states, respectively. These states correspond to the 3p′, 5s, and 4p states in the assignments of Hochmann et al..[15] In the second assignments, the numbers are defined with reference to atomic krypton whose highest occupied orbital (4p) is the same as that for Br. The current assignments of the peaks in Figure 1 are based on the overall shape and the relative intensities of the peaks in the region, rather than on wavelength matches since the resolution of Figure 1 is much higher than the absorption spectra. In addition, the energies for these Rydberg states differ by a few tens to a few hundreds of wavenumbers from the assignments of refs 14 and 15. The fundamental bandwidth of our dye laser at 732 nm is around 0.10−0.16 cm^{-1}. Taking into account the doubling and the subsequent tripling, the VUV bandwidth would be at most 1 cm^{-1}. The wavelength shown is in vacuum and was calibrated using the atomic sulfur absorption line $3s^23p^3(^2D^o)4d\ ^1D_2^\circ \leftarrow 3s^23p^4\ ^1D_2$ at 121.896 nm[22] and, therefore, should be more accurate than those in the previous spectra. Nonetheless, the overall shapes of the PHOFEX spectra closely resemble both the absorption spectra, as well as the photoion spectrum shown in ref 2 in the wavelength region, even though the resolution is much higher in the present case.

B. Velocity Imaging Studies. Images for CH_3^+ and Br^- ions were taken at the wavelengths indicated in Figure 1 by arrows and lines, respectively. These wavelengths were chosen to cover some Rydberg peaks with both s and p characters and valleys where absorption to the continuum should be dominant. The purpose of these studies is to reveal differences, if any, in the dissociation dynamics originating from different excited doorway states which include s and p Rydberg series and valence states. In addition to the marked wavelengths in Figure 1, images for both ions were also collected at 118.22 nm (10.49 eV), where individual Rydberg states cannot be identified due to the

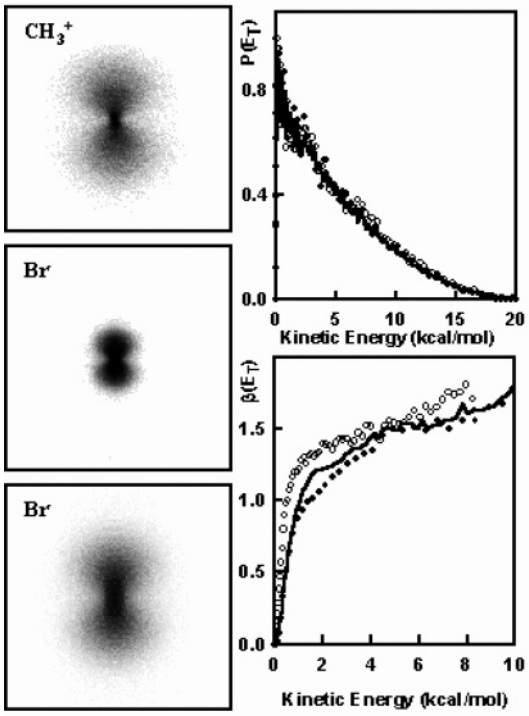

Figure 2. Images of CH_3^+ (upper left) and Br^- (middle left) taken with 2500 V/1730 V voltage setting on the repeller and accelerator, and Br^- (lower left) with 500 V/346 V from ion-pair dissociation of CH_3Br at 118.22 nm. The kinetic energy and angular distributions are shown in the upper right and lower right panels, respectively. Circles and dots are from the detection of CH_3^+ and Br^- at 2500 V/1730 V, respectively. Lines are from the detection of Br^- at 500 V/346 V. Momentum matching is evident. The polarization of 118.22 nm radiation is vertical in the plane and parallel to the detector surface.

congestion in the absorption since this energy is very close to the IE (10.54 eV)[20] of the molecule. At this wavelength, the available energy is ∼2300 cm^{-1} higher than it is in other spectral region of this study. Frequency tripling in Xenon was used to produce 118.22 nm from the 355 nm output of the Nd:YAG laser. The fundamental at 1064 nm has a bandwidth of 1 cm^{-1}. As a result, the bandwidth at 118.22 nm, which is the 9th harmonic of 1064 nm, is expected to be around 9 cm^{-1}. Excitation within this bandwidth is expected to cover multiple Rydberg states of different series. The images, kinetic energy and angular distributions are shown in Figure 2. The results are in good agreement with the previous study at this wavelength.[12]

Images for CH_3^+ at the wavelengths indicated in Figure 1 are shown in Figure 3 except the one at 122.10 nm, which is almost identical to the one at 122.16 nm shown in Figure 3d. All images show strong parallel angular distributions relative to the polarization direction of the UVU laser, regardless of the excitation wavelengths. The image on the strongest peak at 122.16 nm (Figure 3d) reveals layers of distributions. These layers are most likely due to populations in different vibrational levels of CH_3^+, as has been reported recently from the ion-pair dissociation of CH_3Cl at 118 nm,[13,23] where the energy resolution was better, especially in ref 23.

Using the back-projection method,[17] the translational energy and angular distributions of the ion-pair dissociation eq 2 that are derived from the images shown in Figure 3 are presented in Figure 4, where they are arranged in the same order as Figure 3. The population distributions $P(E_T)$ are shown in odd rows with wavelengths, whereas the angular distributions $\beta(E_T)$ are shown immediately below the $P(E_T)$ for the same wavelength.

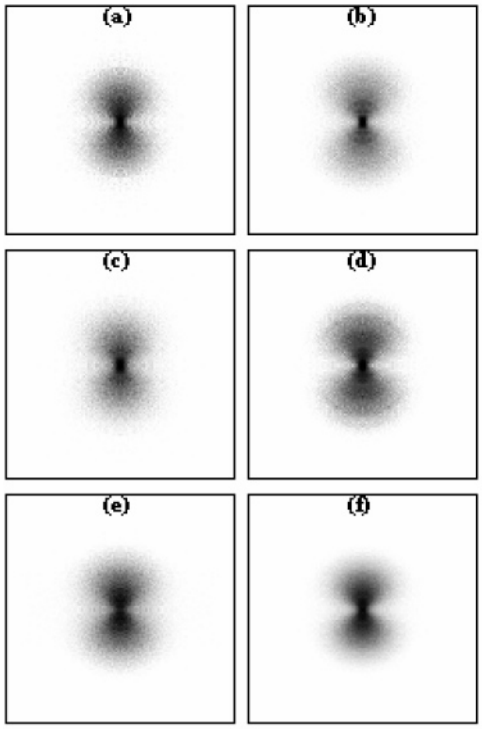

Figure 3. Images for CH_3^+ at different wavelengths: (a) 121.60 nm; (b) 121.83 nm (7p′); (c) 122.04 nm; (d) 122.16 nm (9s); (e) 122.25; (f) 122.43 nm (8p). VUV polarization is vertical in the plane and parallel to the detector surface for all cases.

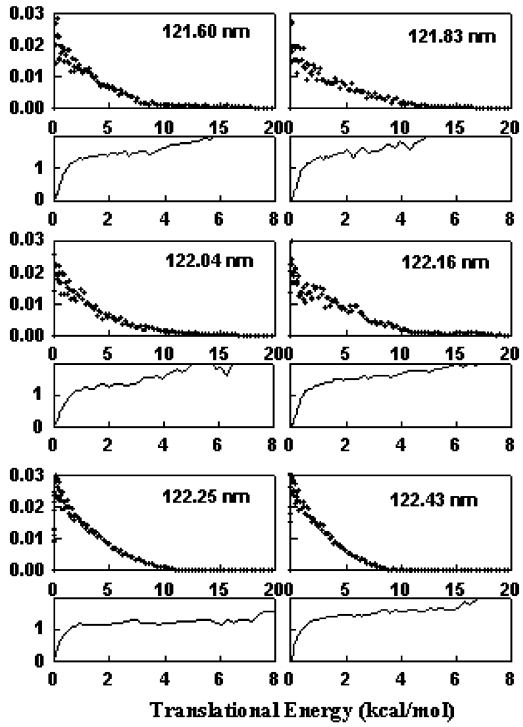

Figure 4. Translational energy, $P(E_T)$ (odd rows), and the angular, $\beta(E_T)$ (even rows), distributions that were derived from CH_3^+ images shown in Figure 3. The wavelengths indicate where the images were taken. $\beta(E_T)$ is shown immediately below $P(E_T)$ at the same wavelength. Note that $\beta(E_T)$ is truncated at 8 kcal/mol since it becomes erratic at higher E_T due to low signal level and noise acquired from 2D to 3D mathematical transform.

It is obvious that these distributions are very similar to those obtained at 118.22 nm, Figure 2, except that the maximum E_T is higher in that case due to more available energy at 118.22 nm.

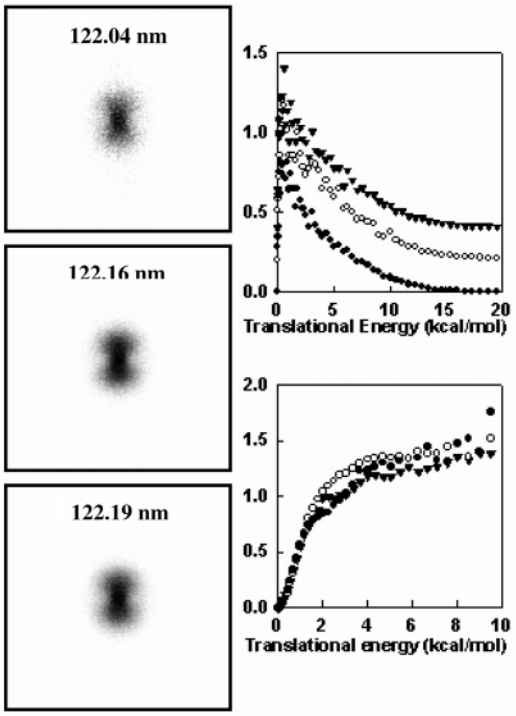

Figure 5. Images of Br^- and the translational energy and angular distributions at three wavelengths. Dots: 122.04 nm; circles: 122.16 nm; and triangles: 122.19 nm. VUV polarization is vertical in the plane and parallel to the detector surface for all cases.

The general shapes of $P(E_T)$ and $\beta(E_T)$ are strikingly similar at the different wavelengths, where different Rydberg states and valence states are excited. The general characteristics of the $P(E_T)$ and $\beta(E_T)$ are that the $P(E_T)$ decreases from a maximum near $E_T = 0$ to zero at high translational energy and the $\beta(E_T)$ increases with E_T in the low kinetic energy region and becomes relatively flat at high E_T. We initially expected to see different dynamics when Rydberg states of ns and np (np′) are populated. Differences are also anticipated from the excitation of Rydberg states and valence states since the former usually should have longer lifetimes that can be revealed from the angular distributions of the products. The figures show, however, that no such differences were observed.

Images of Br^- were collected at three wavelengths as shown in Figure 1; one in the valley at 122.04 nm, one on the 9s peak at 122.16 nm, and one on the shoulder of the 9s peak at 122.19 nm. They are shown in Figure 5 together with the translational energy and angular distributions. As found in the cases of detecting CH_3^+, the similarities in $P(E_T)$ and $\beta(E_T)$ are obvious among these three places, and the general trends are consistent with those shown in Figure 4.

The voltages on the repeller and the accelerator were kept the same when detecting CH_3^+ and Br^-, except that the polarities were changed from positive to negative. Therefore, the magnification factors were the same for both ions. The images for Br^- are smaller than those for CH_3^+ because Br^- is heavier and hence the speed is slower. This is a direct result of linear momentum conservation. Direct comparisons of the $P(E_T)$ and $\beta(E_T)$ obtained from the detection of CH_3^+ and Br^- are given in Figure 6 where both images of CH_3^+ and Br^- were taken at identical wavelengths.

Figure 6 shows the momentum-matched translational energy distributions obtained from the images of CH_3^+ and Br^-, which

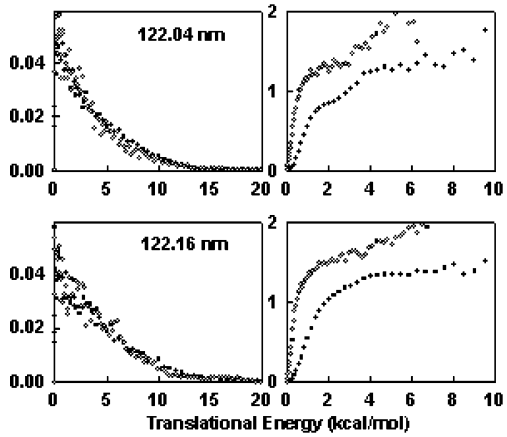

Figure 6. Comparisons of $P(E_T)$, left panel, and $\beta(E_T)$, right panel, obtained from the images of CH_3^+ (circles) and Br^- (dots) taken at identical wavelengths. The $P(E_T)$s show excellent momentum-matching as a result of linear momentum conservation from the pair of fragments. The $\beta(E_T)$s increase fast with E_T at low E_T and become flat at high E_T. The differences in $\beta(E_T)$s derived from the images of CH_3^+ and Br^- ions are due to the finite spatial resolution of detection. See text for details.

proves that these fragments are produced as a pair from the same dissociation. Linear momentum conservation dictates that in the center of mass frame the same total kinetic energies should result from the detection of either fragment. To convert the kinetic energy of CH_3^+, $E_T(CH_3^+)$, to the total energy, the mass factor of $M(CH_3Br)/M(Br)$ should be applied, whereas $M(CH_3Br)/M(CH_3)$ should be used to convert $E_T(Br^-)$ to the total energy. The $\beta(E_T)$s are small in the low E_T region and increase fast with E_T at low E_T and become relatively flat at high E_T. This trend will be discussed in the next section.

At the same E_T, β from Br^- image is smaller than that from CH_3^+. Similar results were obtained at 118.22 nm as Figure 2 shows. Most probably, this is due to the finite spatial resolution of the camera and/or of the phosphor screen. An example is given in Figure 2. The lower left image for Br^- was taken with low voltages on the repeller and the accelerator, which allowed the Br^- ions to cover a larger area on the MCP and hence on the CCD chip of the camera. As shown in the lower right part of Figure 2, the $\beta(E_T)$s from this image increase and get closer to those obtained from the image of CH_3^+ ions.

IV. Discussion

A. Photofragment Excitation. In many cases, ion-pair production efficiencies closely follow the absorption spectra.[2,5] From this observation, it has been suggested that the excitation is initially to populate the Rydberg and nearby valence states and then the molecule crosses over to the ion-pair state.[12] The Rydberg states are considered the doorways through which the curve crossing occurs. It is an appealing mechanism based on the argument that direct excitation to ion-pair states is unlikely because of the absence of structured ion-pair absorption below the dissociation threshold[24] and because of the unfavorable Franck−Condon factors stemming from the large displacement of the ground and the ion-pair states. Further, it is suggested that all of the Rydberg states accessed above the ion-pair dissociation limit are *equally* predissociated to the ion-pair continua since the ion-pair yields mimicked the absorption and no selectivity regarding to Rydberg state doorways was observed.[24]

When the PHOFEX spectra in Figure 1 are compared to the absorption spectra, they also seem to closely follow the absorption, although detailed comparison is impossible because there are no comparable high-resolution absorption spectra. Nonetheless, previous ion-pair efficiency curve[2] with comparable resolution to absorption spectra does suggest that this is the case. One conclusion that could be drawn from this observation is that ion-pair dissociation is one of the major exit channels for the excited states in this energy region. Similar suggestions were made in the cases of I_2 and ICl.[24] The efficiency for the ion-pair channel drops sharply[2] when the photon energy is above the IE of the molecule, because another channel, direct molecular ionization, competes with the ion-pair dissociation channel. In a sense, ion-pair dissociation can be viewed as sub-threshold photoionization, except that the electron is replaced by a heavy anion.

The H channel from photodissociation of CH_3Br has been observed at 121.6 nm by means of high-n Rydberg-atom TOF technique.[25] A bimodal product kinetic energy distribution was found. The fast H atoms were formed from $H + CH_2Br(X)$ channel and the slow H atoms were formed from three-body dissociation channels of $H + H_2 + CBr$ and/or $H + Br + CH_2$. Isotropic angular distributions were found for both the fast and slow channels. No quantum yield was reported at this wavelength, and therefore, it is difficult to assess the relative importance of the neutral channels to the ion-pair channel.

Different types of dipole transitions, i.e., parallel and perpendicular, are expected when Rydberg states with different orbital angular momentum are excited from the neutral ground state of CH_3Br ($^1A_1$). Within the wavelength region covered in Figure 1, ns, np, and np′ Rydberg series are excited. In their I_2 multiccolor resonant enhanced excitation experiments, Ridley et al. found that at a randomly selected transition the shape of the TOF profile of I^+ changed from double-peaked to single-peaked when the probe laser polarization was rotated from parallel to perpendicular to the TOF axis. They suggested that the polarization detection could be used to probe the spectroscopic character of the doorway states from which ion-pair dissociation occurred. This implies that information on the dissociation dynamics is necessary to understand the initially excited states and the couplings between them and the ion-pair states. One of the motivations for the present study on ion-pair formation as a function of wavelength is to reveal possible differences in ion-pair dissociation dynamics originating from different parts of the potential surfaces.

B. Translational Energy Distribution. As shown in Figures 2 and 4, the shapes of kinetic energy distributions all appear very similar to each other at all wavelengths. They all peak near zero kinetic energy and extend almost to the maximum energy available. This is similar to the kinetic energy distribution for simple bond rupture, which forms two neutral radicals on the ground-state surface following internal conversion from the excited state. Direct dissociation from a repulsive state often produces a Gaussian-shaped energy distribution with the most populated products being shifted to high kinetic energy, as a result of the reflection of the ground vibrational state wave function. Such cases include the dissociation of halogenated methanes from their first absorption band, A-band, which results from the promotion of a nonbonding electron to the antibonding σ^* orbital.[26−28]

A direct Franck−Condon transition to the repulsive part of an ion-pair state only occurs at short internuclear distances. At first glance, it does not appear that the observed $P(E_T)$ supports such an excitation process because it is peaked at low translational energies. Although this is true for diatomic molecules, it is not necessarily true for ion-pair states involving

TABLE 1: Energy (kcal/mol) Partitioning at Different Wavelengths of the Ion-Pair Dissociation $CH_3Br + h\nu_{VUV} \rightarrow CH_3^+ + Br^-$

wavelengths (nm)	E_{avail}	$\langle E_T \rangle$	$\langle E_T \rangle / E_{avail}$
118.22	22.9	5.1	0.22
121.60	17.2	3.7	0.22
121.83	15.7	4.0	0.25
122.04	15.3	3.6	0.24
122.16	15.1	4.3	0.28
122.25	14.9	3.1	0.21
122.43	14.5	2.5	0.17

polyatomic molecules since some of the available energy can be tied up in the internal energy of the polyatomic ion. The ion-pair state of methyl bromide is formed by bringing together a methyl cation and a bromine anion. It is highly unlikely that the geometry of the methyl cation is the same as the geometry of the methyl in methyl bromide. A Franck−Condon transition, which reflects the vibrational wave function onto the repulsive part of the ion-pair curve, has to lead to distortion of the geometry of the hydrogen atoms on the carbon atom. Thus, a transition to the repulsive part of the ion-pair state from the ground state has to result in some of the available energy being tied up in the internal energy of the methyl cation. Thus, the shape of the $P(E_T)$ curve can be strongly influenced by this requirement of providing internal energy to the methyl cation.

The main interaction between a positive and a negative charge is Coulombic attraction. Repulsion only comes in at short internuclear separations, and there is no pure repulsive state for ion-pair. In this respect, it is understandable that the kinetic energy distributions have a similar shape at all excitation energies and look like those resulting from the dissociation on the ground-state surface forming neutral fragments. Table 1 lists the available energies E_{avail}, average kinetic energies $\langle E_T \rangle$ and their partitioning $\langle E_T \rangle / E_{avail}$. This latter value ranges from 20 to 30% for all wavelengths. The remaining part of the available energy is retained as the internal energy of CH_3^+. This suggests that there is a fast redistribution of the available energy into this ion, and the process of ion-pair dissociation resembles the kind of process one expects for simple bond rupture. This makes sense because free CH_3^+ ion is planar and CH_3 in CH_3Br is pyramidal. In the ion-pair dissociation of CH_3Cl, Ahmed et al.[13] identified that the umbrella vibrational mode υ_2 is the mostly excited mode, together with some low populations in the combination modes. It is likely that the similar vibrational modes have been excited in the present case of CH_3Br. The similarities in the kinetic energy distributions obtained at different wavelengths suggest that a common mechanism applies to the ion-pair dissociation of CH_3Br in the wavelength region studied.

From the kinetic energy distributions, we can postulate the ion-pair dissociation is analogous to neutral dissociation on the ground-state surface. The potential energy surface described by eq 1 is indeed somehow similar to the ground-state surface, except that for the ion-pair state R_e is larger and the vibrational levels are more densely packed in the potential well. On the other hand, one would expect much less anisotropic angular distribution of fragments produced on the ground state surface since internal conversion and energy redistribution among all degrees of freedom generally take time and tend to wash out the initial molecular alignment along the direction of the laser polarization. In this respect, ion-pair dissociation sharply differs from neutral dissociation.

C. Angular Distribution. In diatomic or linear polyatomic molecules, the angular distribution of photofragments can reveal the nature of the excited state with some certainty. For nonlinear polyatomic molecules, this certainty often vanishes since the transition dipole moment is no longer strictly parallel or perpendicular to the breaking bond. Rather, the angle between the transition dipole moment and the fragment recoil direction determines the degree of anisotropy. If there are more than one product channels, the angular distributions could be entirely different for different channels although they originate from a single electronic transition.[29]

All images shown in this paper at different wavelengths show strong anisotropic distributions. The anisotropy parameters β-(E_T) as a function of E_T are displayed in Figures 2, 4, and 5. These distributions are essentially identical regardless of where the molecule is excited in the absorption spectrum. As pointed out earlier, wavelengths were chosen to excite ns, np, and np′ Rydberg states and the valence states located in the absorption valleys. At 118.22 nm, where the photon energy is very close to the IE of CH_3Br and Rydberg states of different series merge together, excitation will populate different states at the same time given the wide bandwidth (9 cm^{-1}) of the VUV at this wavelength. Even at this wavelength, the angular distribution is similar to those at the longer wavelengths. The transition dipole moment should be changing at different wavelengths when different states are excited. However, the current results show that it is always parallel to the C−Br bond, which implies that transitions leading to the ion-pair final channel have dipole moments parallel to the C_3 axis of the molecule. Out of these possible transitions, we think that the excitation that *directly* populates the ion-pair state of $CH_3^+Br^-$ (A_1 symmetry in the C_{3v} group) may be the dominant transition. Although it is expected that excitation along the C−Br coordinate should result in a smooth PHOFEX spectrum, the peaks shown in Figure 1 may come from favorable Franck−Condon overlaps of other vibrational modes between the ground-state CH_3Br and the ion-pair state $CH_3^+Br^-$. These modes may include the low-frequency rocking and deformation modes of both CH_3Br and $CH_3^+Br^-$. They are not necessarily so unfavorable as the C−Br stretching.

Other examples supporting the direct excitation of ion-pair state come from studies of CH_3Cl, CH_3Br, and C_2H_5Cl at 118.22 nm.[11,12] Because the IEs for these molecules are different, the 118.22 nm photon is expected to excite different states of these molecules. And yet, the ion-pair products from these molecules all show strong parallel angular distributions. The most appealing explanation for these results would be, again, the direct population of the ion-pair states from the ground states, which results from parallel transitions of $A_1 \rightarrow A_1$ for CH_3Cl and CH_3Br and $A' \rightarrow A'$ for C_2H_5Cl. There is no reason to doubt that ion-pair states can be directly populated by single photon excitation, which would reach the inner wall of the ion-pair states. In fact, one would expect favorable Franck−Condon overlaps between the ground vibrational state of CH_3Br (X) and the high vibrational states of $CH_3^+Br^-$ since the vibrational wave functions of $CH_3^+Br^-$ have the largest amplitude near the classical turning point. It is pointed out in ref 1 that optically allowed transitions of X → ion-pair will have much larger transition dipoles at small separations than X → Rydberg transitions of the same polarization.

If excitation of CH_3Br in this spectral region populates a Rydberg state or a valence state and these states subsequently cross over to the ion-pair state, then we have to assume that *all* transition dipole moments to the ns, np, np′, and valence states at the different wavelengths must be parallel to the C−Br bond in order to explain the current results. This assumption is certainly questionable since the symmetries of the Rydberg states converging to different ion core states are different,[25] which

should give rise to transition dipole moments oriented at different directions that would in turn result in different fragment angular distributions. This clearly contradicts the current experimental observations. In the present case where the interaction of the ion-pair state with the nearby Rydberg or valence states is likely to be strong, an adiabatic description of the state seems to be more suitable for defining the system because the interaction matrix elements would be too large to be considered as the perturbation term in the Hamiltonian. In this adiabatic description, the molecule stays in the same electronic eigenstate but the underlying configuration may change.[1] This may help to understand the strong parallel angular distributions at different wavelengths observed in the present study since the electronic transition dipole moment from CH_3Br (X, A_1) $\rightarrow$ $CH_3^+Br^-$ (A_1) would be parallel to the C−Br bond.

The proposed mechanism of direct ion-pair excitation should be considered only applicable to the CH_3Br molecule in the energy region covered by the present study. This could be due to the complexity of the interactions between the ion-pair state and the nearby valence and Rydberg states. In recent work on the ion-pair dissociation of CH_3F, Suits and co-workers[30] observed changes in the angular distribution going from moderate perpendicular ($\beta = -0.18$) to near isotropic ($\beta = -0.08$) and then to moderate parallel ($\beta = 0.23$) when the molecule was excited at 13.52, 13.68, and 13.95 eV, respectively. They have successfully modeled this change in the anisotropy by assuming that the Rydberg states of $3s(a_1)$ and $3p(a_1)$ (both with $^2E_{1/2}$ ion core) were excited by promoting an electron from the $5a_1$/1e valence orbitals. The polarization from the $5a_1$ orbital to the 3s and 3p is parallel, and that from the 1e orbital is perpendicular. The computed β was determined by the relative transition strengths and the polarizations of the four transitions involved. The success of matching the observed anisotropy with the theoretical estimates does suggest that the Rydberg levels are initially excited in CH_3F. The change of anisotropy is also what we initially expected to find in this study. The difference between CH_3F and CH_3Br may be due to the differences in the strengths and positions of the state mixing in the two molecules and in the importance of spin−orbit coupling in them.

In the VUV laser excitation study on the ion-pair formation of I_2 and ICl, Lawley et al. also found that the PHOFEX spectra of I^+, I^-, and Cl^- ions coincided with the absorption spectra. They proposed that the molecules were first excited to Rydberg states that were then *equally* predissociated by the ion-pair states, and that ion-pair dissociation was the dominant exit channel.[24] It appears to be too much of a coincidence that all assigned Rydberg states including ns, np, nd, and nf series are equally coupled to ion-pair continua and hence equally predissociated by the ion-pair continua. It would be premature to say that the ion-pair states are directly populated for these two molecules until data on the fragment energy and angular distributions from the different Rydberg states become available. Nonetheless, it is certainly a possibility.

In detecting the H-atom channels from the dissociation of CH_3Br at 121.6 nm, Amaral et al.[25] found that the angular distributions were isotropic for both the fast and the slow H-atom channels. The single photon dipole allowed transitions include the $A_1 \rightarrow A_1$ with the transition dipole being parallel to C−Br bond and the $A_1 \rightarrow E$ with the transition dipole being perpendicular to the C−Br bond. In the fast dissociation limit for the H-atom channel, the parallel transition will result in a $\beta = -0.64$, whereas $\beta = 0.33$ for the perpendicular transition. The authors proposed that the $\beta \approx 0$ could be due to mixed and averaged contributions from both the A_1 and the E excited states or due to slow (relative to the rotational period) dissociation. However, the image shown in Figure 3a at 121.60 nm exhibits strong anisotropic angular distribution, consistent with an $A_1 \rightarrow A_1$ transition and a short excited-state lifetime. To rationalize the present observation with the results of ref 25, a fast coupling must be invoked between the initial excited state and other neutral states that undergo slow dissociation producing H atoms.

The $\beta(E_T)$ distributions for CH_3^+ and Br^- shown in Figures 2, 4, 5, and 6 show that in the low E_T region β increases with E_T and then becomes relatively flat at medium to high E_T. This trend of $\beta(E_T)$ mainly arises from the rotation of the molecules that were excited. When the molecule breaks apart, the fragments possess a tangential velocity that is perpendicular to the recoil velocity. The angular distribution will be determined by the composite velocity of the tangential and recoil velocities, and will be degraded in the center of mass frame relative to that resulting from rotation-less molecules. The deviation from the initial recoil velocity will give rise to a less anisotropic angular distribution. Since this deviation is larger for the slow fragments than for the fast fragments, a larger decrease of β from the limiting value will be observed for the slow fragments than for the fast fragments. The other reason for this $\beta(E_T)$ trend is related to the finite spatial resolution of the camera and/or the phosphor screen, which has been presented earlier in the paper.

V. Conclusions

Ion-pair dissociation dynamics of CH_3Br have been studied as a function of wavelength. The photofragment excitation spectra closely resemble the absorption spectra. No differences in dynamics were found at different wavelengths, where the previously reported different series of Rydberg states (ns, np, and np′) and valence states were excited by the VUV photons. These results lead us to conclude that in the energy region studied the major excitation is to *directly* populate the ion-pair state that immediately undergoes fast dissociation. The peaks observed in the PHOFEX spectra could result from favorable Franck−Condon overlaps between vibrational modes other than the C−Br stretching mode. This is contrary to the suggestion that initial excitation is to Rydberg states that act as doorways for the molecule to cross over to ion-pair state, although the lack of absorption spectrum of high-resolution comparable to the PHOFEX spectra makes the current conclusion somewhat speculative.

Acknowledgment. This work was supported by NSF (Grant No. CHE-0100965) and NASA (Grant No. NGA5-12124). We thank Dr. Alexei Stuchebrukhov for helpful discussions.

References and Notes

(1) Lawley, K. P.; Donovan, R. J. *J. Chem. Soc., Faraday Trans.* **1993**, *89*, 1885.
(2) Berkowitz, J. *VUV and Soft X-ray Photoionization*; Becker, U., Shirley, D. A., Eds.; Plenum Press: New York, 1996.
(3) Suzuki, S.; Mitsuke, K.; Imamura, T.; Koyano, I. *J. Chem. Phys.* **1992**, *96*, 7500.
(4) Lawley, K. P.; Ridley, T.; Min, Z.; Wilson, P. J.; Al-Kahali, M. S. N.; Donovan, R. J. *Chem. Phys.* **1995**, *197*, 37.
(5) Ridley, T.; de Vries, M.; Lawley, K. P.; Wang, S.; Donovan, R. J. *J. Chem. Phys.* **2002**, *117*, 7117.
(6) Hu, Q. J.; Melville, T. C.; Hepburn, J. W. *J. Chem. Phys.* **2003**, *119*, 8938.
(7) Martin, J. D. D.; Hepburn, J. W. *Phys. Rev. Lett.* **1997**, *79*, 3154.
(8) Shiell, R. C.; Hu, X. K.; Hu, Q. J.; Hepburn, J. W. *J. Phys. Chem. A* **2000**, *104*, 4339.

(9) Muller-Dethlefs, K.; Schlag, E. W. *Annu. Rev. Phys. Chem.* **1991**, *42*, 109.
(10) Krauss, M.; Walker, J. A.; Dibeler, V. H. *J. Res. Natl. Bur. Stand.* **1968**, *72A*, 281.
(11) Munakata, T.; Kasuya, T. *Chem. Phys. Lett.* **1989**, *154*, 604.
(12) Suto, K.; Sato, Y.; Reed, C. L.; Skorokhodov, V.; Matsumi, Y.; Kawasaki, M. *J. Phys. Chem. A* **1997**, *101*, 1222.
(13) Ahmed, M.; Peterka, D. S.; Regan, P.; Liu, X.; Suits, A. G. *Chem. Phys. Lett.* **2001**, *339*, 203.
(14) Causley, G. C.; Russell, B. R. *J. Chem. Phys.* **1975**, *62*, 848.
(15) Hochmann, P.; Templet, P. H.; Wang, H.-t.; McGlynn, S. P. *J. Chem. Phys.* **1975**, *62*, 2588.
(16) Jackson, W. M.; Xu, D. D. *J. Chem. Phys.* **2000**, *113*, 3651.
(17) Sato, Y.; Matsumi, Y.; Kawasaki, M.; Tsukiyama, K.; Bersohn, R. *J. Phys. Chem.* **1995**, *99*, 16307.
(18) Suto, K.; Sato, Y.; Matsumi, Y.; Kawasaki, M. *J. Phys. Chem. A* **1997**, *101*, 1227.
(19) Xu, D. D.; Price, R. J.; Huang, J. H.; Jackson, W. M. *Z. Phys. Chem.* (Munich) **2001**, *215*, 253.
(20) http://webbook.nist.gov/chemistry/
(21) Blush, J. A.; Chen, P.; Wiedmann, R. T.; White, M. G. *J. Chem. Phys.* **1993**, *98*, 3557.
(22) Huang, J. H.; Xu, D. D.; Stuchebrukhov, A.; Jackson, W. M. *Can. J. Chem.* **2004**, *82*, 885.
(23) Liu, X. H.; Gross, R. L.; Suits, A. G. *Science* **2001**, *294*, 2527.
(24) Lawley, K. P.; Flexen, A. C.; Maier, R. R. J.; Manck, A.; Ridley, T.; Donovan, R. J. *Phys. Chem. Chem. Phys.* **2002**, *4*, 1412.
(25) Amaral, G.; Xu, K.; Zhang, J. *J. Phys. Chem.* **2001**, *105*, 1115.
(26) Xu, D. D.; Francisco, J. S.; Huang, J. H.; Jackson, W. M. *J. Chem. Phys.* **2002**, *117*, 2578.
(27) Huang, J. H., Xu, D. D.; Francisco, J. S.; Jackson, W. M. *J. Chem. Phys.* **2003**, *119*, 3661.
(28) Lee, S.-H.; Jung, K.-H. *Chem. Phys. Lett.* **2001**, *350*, 306.
(29) Xu, D. D.; Huang, J. H.; Francisco, J. S.; Hansen, J. C.; Jackson, W. M. *J. Chem. Phys.* **2002**, *117*, 7483.
(30) Li, W.; Lucchese, R. R.; Doyuran, A.; Wu, Z.; Loos, H.; Hall, G. E.; Suits, A. G. *Phys. Rev. Lett.* **2004**, *92*, 83002.